AIAA JOURNAL
Vol. 30, No. 9, September 1992

# Effect of Pressure Gradient on the Stability of Compressible Boundary Layers

Y. H. Zurigat,* A. H. Nayfeh,† and J. A. Masad‡
*Virginia Polytechnic Institute and State University, Blacksburg, Virginia 24061*

**An investigation into the influence of pressure gradient (wall shaping) on the stability of compressible boundary layers is presented. The steady, compressible, nonsimilar boundary-layer equations are solved with a potential flow velocity distribution corresponding to a power law edge Mach number distribution. The stability of the mean flow is investigated using the small-disturbance compressible linear stability theory. The results indicate that two-dimensional second-mode (Mack) waves can be stabilized with pressure gradient. However, the effectiveness of the pressure gradient on the natural laminar flow control of two-dimensional second-mode waves decreases at hypersonic speeds. The maximum growth rate varies almost linearly with the pressure gradient level. The effect of pressure gradients on stabilizing three-dimensional first-mode waves is much larger than their effect on stabilizing two-dimensional first-mode waves.**

## I. Introduction

THE process of transition from laminar to turbulent flow still lacks detailed understanding. However, it is believed that the origin of many turbulent flows is in the laminar flow instability to various external and internal disturbances. Therefore, small-disturbance stability theory has been extensively used to evaluate the effectiveness of proposed natural laminar flow (NLF) as well as laminar flow control (LFC) concepts. The factors that influence the stability of incompressible and compressible boundary-layer flows include pressure gradients, wall roughness, heating or cooling, freestream turbulence, suction or blowing, Coriolis forces and streamwise curvature, and radiated acoustic noise.

The effect of pressure gradients (wall shaping) on laminar flow instability is of particular interest because it is a passive device for controlling the boundary layer. Previous investigations,[1,2] have shown that a favorable pressure gradient stabilizes incompressible boundary layers while adverse pressure gradients produce an opposite effect. The basis for this behavior was established through inviscid analyses that resulted in the well-known Rayleigh criterion regarding the presence of inflection points: profiles with inflection points are unstable. Flows with adverse pressure gradients are known to have inflection points. Reported[3] flight-test data indicate an increase in the transition Reynolds number with an increasingly favorable pressure gradient.

The stability of compressible boundary layers is more complicated than the stability of incompressible boundary layers because of the existence of multiple modes of instability in the former case as opposed to a single instability mode in the latter case. Consequently, factors that have a stabilizing effect on incompressible boundary layers may have a destabilizing effect on compressible boundary layers. Continuous cooling, for instance, was found[4-7] to stabilize first-mode waves and destabilize second-mode (Mack) waves (the latter are dominant at high Mach numbers), whereas continuous heating was found to stabilize second-mode waves. However, very frequently material limits make wall heating impractical for laminar flow control. Moreover, the effect of continuous heat transfer on the first and second modes of instability of boundary layers was found to diminish at high Mach numbers.[8] Wall suction, on the other hand, stabilizes both first- and second-mode waves. However, it was shown[9,10] that the effectiveness of suction diminishes greatly for high Mach numbers. For more details the reader is referred to the reviews[11,12] on compressible boundary-layer stability.

The effect of pressure gradients on the stability of compressible boundary layers requires further study. Few studies have appeared in the literature. Shapiro[13] indicated that the effect of pressure gradients on the value of the critical Reynolds number decreases with increasing Mach number. The same study also concluded that the stabilizing effect of pressure gradients decreases with increasing Mach number for an insulated wall. Weil[14] showed that the effect of favorable pressure gradients on the stability is not large for a Mach number of 4 but extremely pronounced at the lower supersonic Mach number of 1.5. Malik[7] concluded that favorable pressure gradients stabilize second-mode waves by reducing the peak amplification rate. He also found that favorable pressure gradients shift the peak amplification to a higher frequency and decrease the band of frequencies receiving amplification.

Malik[7] used a viscous stability analysis similar to the one used in this paper. However, Malik[7] used a self-similar solution to calculate the mean flow. As pointed out by Malik,[7] this is questionable, since self-similar solutions do not exist for the investigated conditions. Moreover, each of the three cases investigated in his study was restricted to a single Mach number, a single Reynolds number, and favorable pressure gradients only. The purpose of this paper is to document a detailed study of the influence of wall shaping on the stability of compressible boundary layers based on mean flows calculated by using nonsimilar boundary layers.

## II. Mean Flow

The mean flow investigated in this study is governed by the two-dimensional compressible boundary-layer equations.[15] Using the Levy-Lees variables

$$\xi(x)=\int_0^x u_e\,dx \tag{1}$$

$$\eta(x,y)=\frac{\sqrt{Re}\,u_e}{\sqrt{2\xi}}\int_0^y \rho\,dy \tag{2}$$

Presented as Paper 90-1451 at the AIAA 21st Fluid Dynamics, Plasma Dynamics, and Lasers Conference, Seattle, WA, June 18-20, 1990; received Oct. 22, 1990; revision received Feb. 20, 1991; accepted for publication Feb. 26, 1991. 

*Currently Assistant Professor, Mechanical Engineering Department, University of Jordan, Amman, Jordan.

†University Distinguished Professor, Department of Engineering Science and Mechanics. Fellow AIAA.

‡Currently Research Scientist, High Technology Corporation, Hampton, VA.

one can write the nonsimilar boundary-layer equations of mass, momentum, and energy. These equations are presented here for completeness and later reference:

$$2\xi\frac{\partial F}{\partial \xi}+\frac{\partial V}{\partial \eta}+F=0 \tag{3}$$

$$2\xi F\frac{\partial F}{\partial \xi}+V\frac{\partial F}{\partial \eta}-\frac{\partial}{\partial \eta}\left(l\frac{\partial F}{\partial \eta}\right)+\beta_0(F^2-Q)=0 \tag{4}$$

$$2\xi F\frac{\partial Q}{\partial \xi}+V\frac{\partial Q}{\partial \eta}-\frac{1}{Pr}\frac{\partial}{\partial \eta}\left(l\frac{\partial Q}{\partial \eta}\right)-(\gamma-1)M_\infty^2\frac{u_e^2}{T_e}l\left(\frac{\partial F}{\partial \eta}\right)^2=0 \tag{5}$$

where

$$F=\frac{u}{u_e},\qquad Q=\frac{T}{T_e},\qquad l=\rho\mu \tag{6a}$$

$$V=\frac{\sqrt{2\xi}}{u_e}\left[\sqrt{Re}\,\rho v+\frac{\partial \eta}{\partial x}\sqrt{2\xi}F\right] \tag{6b}$$

$$\beta_0=\frac{2\xi}{u_e}\frac{du_e}{d\xi} \tag{6c}$$

The boundary conditions for an adiabatic wall are

$$F=0\quad\text{and}\quad\frac{\partial Q}{\partial \eta}=0\quad\text{at}\quad\eta=0 \tag{7a}$$

$$V=\frac{\sqrt{2\xi Re}}{u_e}\rho(0)v_w\quad\text{at}\quad\eta=0 \tag{7b}$$

In the freestream, the boundary conditions are

$$F\to 1\quad\text{and}\quad Q\to 1\quad\text{as}\quad\eta\to\infty \tag{7c}$$

In Eqs. (1-7), $\rho$, $\mu$, $u$, $v$, and $T$ are the nondimensional density, dynamic viscosity, streamwise normal velocity component, and temperature, respectively; $M_\infty$ is the freestream Mach number; and

$$Re=\frac{u_\infty^* L^*\rho_\infty^*}{\mu_\infty^*},\qquad Pr=\frac{\mu_\infty^* C_p^*}{\kappa_\infty^*},\qquad\text{and}\qquad\gamma=\frac{C_p^*}{C_v^*} \tag{8}$$

where the asterisk denotes a dimensional quantity, and $C_p^*$ and $C_v^*$ are, respectively, the gas specific heat coefficients at constant pressure and constant volume. Here, lengths are normalized with respect to a reference length $L^*$; the temperature, viscosity, density, and velocity are normalized with respect to their freesteam values $T_\infty^*$, $\mu_\infty^*$, $\rho_\infty^*$, and $u_\infty^*$, respectively. The subscript $e$ refers to conditions at the edge of the boundary layer.

Among the pressure gradients encountered are Howarth's linearly retarded and accelerated, Goland's accelerated, and constant pressure gradient (Falkner-Skan type) flows. The outer velocity distributions for these flows are given, respectively, by

$$u_e=u_e^*/u_\infty^*=1+ax \tag{9}$$

$$u_e=u_e^*/u_\infty^*=3x(1-x^2) \tag{10}$$

$$u_e=u_e^*/u_\infty^*=x\left(\frac{\beta_0}{2-\beta_0}\right) \tag{11}$$

One may also employ a certain boundary-layer edge Mach number distribution of the form

$$M_e=cx^n \tag{12}$$

where $c$ is a constant. In this study we focus on pressure gradients with potential flow distributions corresponding to Eq. (12) only.

Equations (3-5), along with the boundary conditions (7), are solved using a finite difference method with a Newton-Raphson linearization. The formulation follows that described by Blottner.[16] A nonuniform grid spacing in the streamwise and normal directions is incorporated into the present formulation. The grid spacing is chosen so that the resulting solution is grid independent. The special case of self-similar boundary layers is obtained by dropping the leading terms in Eqs. (3-5). This self-similar solution is then used to start its nonsimilar counterpart.

It should be noted that the self-similar solution is for the zero pressure gradient case. Self-similar solutions for nonzero pressure gradients are rare in compressible boundary layers. It was shown[17,18] that similarity is secured only under restricted conditions; the most realistic condition demands that the Prandtl number be equal to unity. Equations (3-5) do not reduce to a self-similar form for a nonzero value of $\beta_0$ by merely neglecting the leading terms. For the power law edge Mach number distribution investigated in this study, the nonsimilar equations (3-5) have been solved with the edge velocity distribution $u_e$ derived from Eq. (12).

The momentum and energy equations are coupled. Also, the variation of $l$ across the boundary layer can be quite large, ranging over an order of magnitude, especially at hypersonic speeds. Therefore, these equations are solved iteratively while updating $l$, $F$, $V$, and $Q$ until the accumulated change, over all points, in either the temperature or the velocity is within a preset tolerance. The adiabatic wall temperature $Q_w$ is calculated from the adiabatic wall condition $\partial Q/\partial \eta|_{\eta=0}=0$, which is expressed in a three-point one-sided finite difference analog. The wall temperature calculated in this manner is then updated by iteratively solving the energy equation until a vanishingly small change in $Q_w$ is achieved. To speed up the convergence, we have calculated the initial guess from the relationship

$$Q_w=1+\tfrac{1}{2}(\gamma-1)M_e^2\sqrt{Pr} \tag{13}$$

The edge temperature is computed using the isentropic flow relation

$$T_e=\frac{T_e^*}{T_\infty^*}=1+\tfrac{1}{2}(\gamma-1)M_\infty^2[1-u_e^2] \tag{14}$$

The density and viscosity at the edge of the boundary layer are calculated by using the equation of state and the Sutherland's formula, respectively, as

$$\rho_e=\frac{\rho_e^*}{\rho_\infty^*}=T_e^{1/(\gamma-1)} \tag{15}$$

$$\mu_e=\frac{\mu_e^*}{\mu_\infty^*}=T_e^{1.5}\left(1+\frac{110.4}{T_\infty^*}\right)\Big/\left(T_e+\frac{110.4}{T_\infty^*}\right) \tag{16}$$

The pressure gradient parameter $\beta_0$ is calculated by using Eq. (6c) with $u_e$ computed from Eq. (12) as

$$\mu_e=\frac{\mu_e^*}{\mu_\infty^*}=\frac{M_d}{M_\infty}T_e^{1/2}x^n \tag{17}$$

where $M_d$ is the desired edge Mach number at $x=1.0$ where the stability calculations are performed. In these calculations an initial zero pressure gradient region of length $x_0=0.2$ is used. Then the flow is assumed to undergo either an isentropic compression or an isentropic expansion to the desired value $M_d$ of $M_e$ at $x=1.0$. Moreover, we keep the freestream temperature $T$ the same so that the viscosity coefficient will be the same, as shown in Eq. (16). Furthermore, by keeping $U_\infty^*$ and varying $L^*$, we keep the Reynolds number the same at $x=1.0$ where the calculations are performed. This allows a direct

comparison between the results obtained by using favorable and adverse pressure gradients at the same conditions ($M_e$ and stability Reynolds number).

For the potential flow velocity distribution given by Eq. (17), Fig. 1a shows the streamwise edge Mach number distribution for different values of $n$. In this case positive (negative) values indicate favorable (unfavorable) pressure gradients. The corresponding variation of $\beta_0$ with streamwise location is shown in Fig. 1b. We note that $\beta_0$ is discontinuous at $x_0$ due to the change in the slope of $Me$. However, this discontinuity has very little influence on the stability calculations because they are performed at locations far downstream from this discontinuity. Moreover, the dependence of $\beta_0$ on $x_0$ is very weak. For example, at $M_\infty = 4.5$ and $n = -0.2$, $\beta_0 = -0.0813$ when $x_0 = 0.2$ and $\beta_0 = -0.08157$ when $x_0 = 0.05$. The velocity and temperature distributions across the boundary layer at the location of interest ($x = 1.0$) are shown in Figs. 2 and 3.

## III. Stability Analysis

The linear quasiparallel three-dimensional compressible stability problem of the calculated two-dimensional mean flow is derived by superimposing a small disturbance on the mean flow to obtain the total-flow quantities in the form

$$\hat{q}(x, y, z, t) = q_m(y) + q(x, y, z, t) \tag{18}$$

where $q$ represents $u$, $v$, $w$, $\rho$, $p$, $\mu$, and $T$; the circumflex represents the total-flow quantities; and the subscript $m$ indicates the mean-flow quantities. The quasiparallel flow assumption neglects the normal velocity as well as the streamwise variations of the mean velocities, temperature, pressure, and density. Thus,

$$u_m = u_m(y), \quad v_m = 0, \quad w_m = w_m(y), \quad T_m = T_m(y) \tag{19}$$

Also, because the mean flow studied is two dimensional, $w_m = 0$. In the boundary layers, $P_m = P_m(x) = P_e$. The nondimensional presure $P_c$ at the edge of the boundary layer is given by

$$P_e = \frac{P_e^*}{\rho_e^* u_e^{*2}} = \frac{1}{\gamma M_e^2} \tag{20}$$

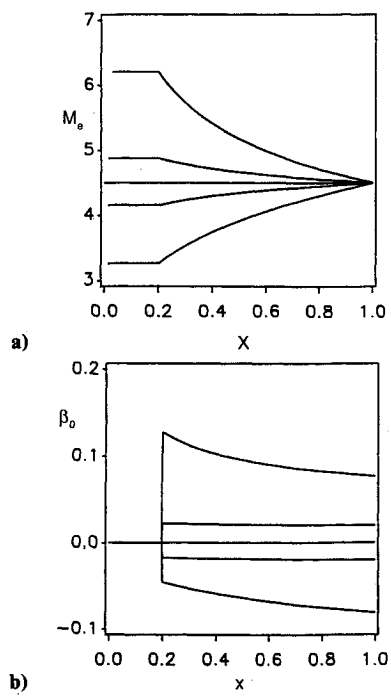


**Fig. 1 Streamwise distributions: a) of boundary-layer edge Mach number ($M_e$); b) of pressure-gradient parameter ($\beta_0$) for different degrees of compression and expansion terminating at $M_e = 4.5$. The values of $n$, proceeding downward, are −0.2, −0.05, 0.0, 0.05, and 0.2.**

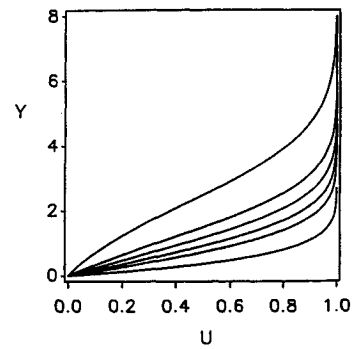


**Fig. 2 Velocity distributions across the boundary layer for different pressure gradient parameters ($M_e = 4.5$ at $x = 1.0$). The values of $n$, proceeding downward, are −0.2, −0.1, −0.05, 0.0, 0.05, and 0.2.**

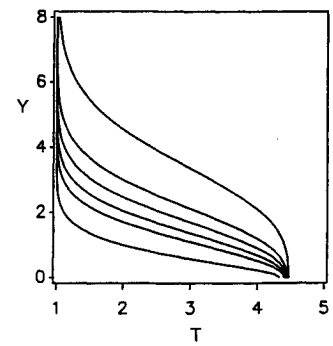


**Fig. 3 Temperature distributions across the boundary layer for different pressure gradient parameters ($M_c = 4.5$ at $x = 1.0$). The values of $n$, proceeding downward, are −0.2, −0.1, −0.05, 0.0, 0.05, and 0.1.**

The Prandtl number $Pr$ is assumed to be constant. Substituting Eqs. (18–20) into the compressible Navier-Stokes equations, subtracting the mean-flow quantities because they satisfy the Navier-Stokes equations, invoking the quasi-parallel-flow assumption, and linearizing with respect to $q$, we obtain the disturbance equations:

$$\frac{\partial \rho}{\partial t} + \rho_m \frac{\partial u}{\partial x} + u_m \frac{\partial \rho}{\partial x} + \frac{\partial}{\partial y}(\rho_m v) + \rho_m \frac{\partial w}{\partial z} = 0 \tag{21}$$

$$\rho_m\left(\frac{\partial u}{\partial t} + u_m \frac{\partial u}{\partial x} + v \frac{du_m}{dy}\right) = -\frac{\partial p}{\partial x} + \frac{1}{R}\left\{\mu_m \frac{\partial}{\partial x}\left(r \frac{\partial u}{\partial x} + m \frac{\partial v}{\partial y} + m \frac{\partial w}{\partial z}\right) + \frac{\partial}{\partial y}\left[\mu_m\left(\frac{\partial u}{\partial y} + \frac{\partial v}{\partial x}\right) + \mu \frac{du_m}{dy}\right] + \mu_m \frac{\partial}{\partial z}\left(\frac{\partial w}{\partial x} + \frac{du}{dz}\right)\right\} \tag{22}$$

$$\rho_m\left(\frac{\partial v}{\partial t} + u_m \frac{\partial v}{\partial x}\right) = -\frac{\partial p}{\partial y} + \frac{1}{R}\left\{\frac{\partial}{\partial x}\left[\mu_m\left(\frac{\partial u}{\partial y} + \frac{\partial v}{\partial x}\right) + \mu \frac{du_m}{dy}\right] + \frac{\partial}{\partial y}\left[\mu_m\left(m \frac{\partial u}{\partial x} + r \frac{\partial v}{\partial y} + m \frac{\partial w}{\partial z}\right)\right] + \mu_m \frac{\partial}{\partial z}\left(\frac{\partial v}{\partial z} + \frac{\partial w}{\partial y}\right)\right\} \tag{23}$$

$$\rho_m\left(\frac{\partial w}{\partial t}+u_m\frac{\partial w}{\partial x}\right)=-\frac{\partial p}{\partial z}+\frac{1}{R}\left\{\mu_m\frac{\partial}{\partial x}\left(\frac{\partial w}{\partial x}+\frac{\partial u}{\partial z}\right)\right.$$

$$\left.+\frac{\partial}{\partial y}\left[\mu_m\left(\frac{\partial v}{\partial z}+\frac{\partial w}{\partial y}\right)\right]+\mu_m\frac{\partial}{\partial z}\left(m\frac{\partial u}{\partial x}+m\frac{\partial v}{\partial y}+r\frac{\partial w}{\partial z}\right)\right\} \tag{24}$$

$$\rho_m\left[\frac{\partial T}{\partial t}+u_m\frac{\partial T}{\partial x}+v\frac{\mathrm{d}T_m}{\mathrm{d}y}\right]=(\gamma-1)M_e^2\left[\frac{\partial p}{\partial t}+u_m\frac{\partial p}{\partial x}+\frac{1}{R}\phi\right]$$

$$+\frac{1}{RPr}\left\{\mu_m\frac{\partial^2 T}{\partial x^2}+\frac{\partial}{\partial y}\left(\mu_m\frac{\partial T}{\partial y}+\mu\frac{\mathrm{d}T_m}{\mathrm{d}y}\right)+\mu_m\frac{\partial^2 T}{\partial z^2}\right\} \tag{25}$$

$$\phi=2\mu_m\left(\frac{\partial u}{\partial y}+\frac{\partial v}{\partial x}\right)\frac{\mathrm{d}u_m}{\mathrm{d}y}+\mu\left(\frac{\mathrm{d}u_m}{\mathrm{d}y}\right)^2 \tag{26}$$

The constants $r$ and $m$ are given by

$$r=m+2 \qquad \text{and} \qquad m=\frac{\lambda_m}{\mu_m} \tag{27}$$

where $\lambda_m$ is the second coefficient of viscosity, and $m=-0.2/3.0$. The local Reynolds number $R$ in Eqs. (22–25) is based on a reference length $\delta_r^*=\sqrt{\nu_e^* x_r^*/u_e^*}$, where $x_r^*$ is the distance from the leading edge to the location where the stability calculations are performed. Hence,

$$R=\frac{u_e^*\delta_r^*}{\nu_e^*}=\sqrt{\frac{u_e^* x_r^*}{\nu_e^*}}=\sqrt{Re_x} \tag{28}$$

Velocities are normalized with respect to the boundary-layer edge velocity $u_e^*$, lengths are normalized with respect to $\delta_r^*$, and time is normalized with respect to $\delta_r^*/u_e^*$.

The boundary conditions are

$$u=v=w=T=0 \qquad \text{at} \qquad y=0 \tag{29}$$

$$u,\ v,\ w,\ T,\ p \qquad \text{are bounded as} \qquad y\to\infty \tag{30}$$

It is assumed that $\mu$ is a function of temperature only. Hence, using a Taylor series expansion, we have

$$\mu=T\frac{\mathrm{d}\mu_m}{\mathrm{d}T}(T_m)=\mu_m' T \tag{31}$$

Moreover, the linearized disturbance equation of state takes the form

$$p/p_m=T/T_m+\rho/\rho_m \tag{32}$$

The solution is sought in the form of three-dimensional traveling waves as

$$[u,\ v,\ p,\ T,\ w]=[\zeta_1(y),\ \zeta_3(y),\ \zeta_4(y),\ \zeta_5(y),\ \zeta_7(y)]$$

$$\exp[i(\textstyle\int\alpha\,\mathrm{d}x+\beta z-\omega t)] \tag{33}$$

where $\alpha$ and $\beta$ are the streamwise and spanwise wave numbers, respectively, and $\omega$ is the frequency. Substituting Eq. (33) into Eqs. (21–26) and using Eqs. (31) and (32), we obtain the eigenvalue problem:

$$D\zeta_3+i\alpha\zeta_1-\frac{DT_m}{T_m}\zeta_3+i(\alpha u_m-\omega)\left(\gamma M_e^2\zeta_4-\frac{\zeta_5}{T_m}\right)+i\beta\zeta_7=0 \tag{34}$$

$$i(\alpha u_m-\omega)\zeta_1+\zeta_3 Du_m+i\alpha T_m\zeta_4-\frac{T_m}{R}\{-\mu_m(r\alpha^2+\beta^2)\zeta_1$$

$$-\alpha\beta\mu_m(m+1)\zeta_7+i(m+1)\alpha\mu_m D\zeta_3+\mu_m' D\zeta_1 DT_m$$

$$+i\alpha\mu_m'\zeta_3 DT_m+\mu_m D^2\zeta_1+D(\mu_m' Du_m)\zeta_5$$

$$+\mu_m' Du_m D\zeta_5\}=0 \tag{35}$$

$$i(\alpha u_m-\omega)\zeta_3+T_m D\zeta_4-\frac{T_m}{R}\{i(m+1)\alpha\mu_m D\zeta_1$$

$$+im\alpha\mu_m'\zeta_1 DT_m-(\alpha^2+\beta^2)\mu_m\zeta_3+r\mu_m' D\zeta_3 DT_m$$

$$+im\beta\mu_m'\zeta_7 DT_m+i\alpha\mu_m' Du_m\zeta_5+r\mu_m D^2\zeta_3$$

$$+i(m+1)\beta\mu_m D\zeta_7\}=0 \tag{36}$$

$$i(\alpha u_m-\omega)\zeta_7+i\beta T_m\zeta_4-\frac{T_m}{R}\{-(m+1)\alpha\beta\mu_m\zeta_1$$

$$+i\beta\mu_m'\zeta_3 DT_m+i(m+1)\beta\mu_m D\zeta_3-\mu_m(\alpha^2+r\beta^2)\zeta_7$$

$$+\mu_m' D\zeta_7 DT_m+\mu_m D^2\zeta_7\}=0 \tag{37}$$

$$i(\alpha u_m-\omega)\zeta_5+\zeta_3 DT_m-i(\gamma-1)T_m M_e^2(\alpha u_m-\omega)\zeta_4$$

$$-(\gamma-1)M_e^2\frac{T_m}{R}[2Du_m\mu_m(D\zeta_1+i\alpha\zeta_3)+\mu_m'(Du_m)^2\zeta_5]$$

$$-\frac{T_m}{RPr}[-\mu_m(\alpha^2+\beta^2)\zeta_5+D(\mu_m D\zeta_5)$$

$$+D(\mu_m' DT_m\zeta_5)]=0 \tag{38}$$

where $D\equiv\mathrm{d}/\mathrm{d}y$

$$\zeta_1=\zeta_3=\zeta_5=\zeta_7=0 \qquad \text{at} \qquad y=0 \tag{39}$$

$$\zeta_n \qquad \text{are bounded as} \qquad y\to\infty \tag{40}$$

Equations (34–40) constitute an eigenvalue problem connecting $\alpha$, $\beta$, $\omega$ (in general these are complex), and $R$, yielding the complex dispersion relation

$$F(\alpha,\ \beta,\ \omega,\ R)=0$$

Because the mean flow is two dimensional, the nondimensional spanwise wave number $\beta$ is real and is given by

$$\beta=\beta^*\delta_r^*=\beta^*\nu_e^* R/u_e^*$$

In this work the case of spatial stability is considered so that $\omega$ is real and $\alpha=\alpha_r+i\alpha_i$ is complex. Hence, the complex dispersion relation provides two real equations connecting $\alpha_r$ and $\alpha_i$, with the other parameters being specified. The nondimensional frequency $\omega=\omega_r^*\delta_r^*/u_e^*$ is replaced by the nondimensional frequency $F$ as $\omega=RF$, where $F=\omega^*\nu_e^*/u_e^{*2}$. The dimensional circular frequency $\omega^*$ remains unchanged as the wave propagates downstream. Hence, $F$ varies with the edge conditions.

## IV. Solution Technique

The eigenvalue problem is solved by using the finite difference code DBVPFD coupled with a Newton-Raphson iteration scheme. This code is an IMSL subroutine that is based on PASVA3 (Ref. 19). The code solves linear or nonlinear two-point boundary-value problems using a variable-order, variable-step finite difference method with deferred correction.

To use DBVPFD code, we have converted the system of Eqs. (34–38) into a system of first-order equations by letting

$$\zeta_2 = D\zeta_1, \qquad \zeta_6 = D\zeta_5, \qquad \text{and} \qquad \zeta_8 = D\zeta_7 \tag{41}$$

Then the eigenvalue problem becomes

$$D\zeta = A(y)\zeta \tag{42}$$

subject to the boundary conditions

$$\zeta_1 = \zeta_3 = \zeta_5 = \zeta_7 = 0 \qquad \text{at} \qquad y = 0 \tag{43}$$

$$\zeta_n \qquad \text{are bounded as} \qquad y \to \infty \tag{44}$$

where $\zeta = \{\zeta_1, \zeta_2, \ldots, \zeta_\infty\}^T$, and the elements $a_{ij}$ of the matrix $A(y)$ are given in the Appendix.

Because the lengths in the stability calculations are normalized with respect to $\delta_r^*$, the mean-flow normal coordinate is transformed into the stability coordinate $y$ as

$$y = \frac{y_m^*}{\delta_r^*} = \frac{\sqrt{2\xi/x}}{\sqrt{\mu_e \rho_e u_e}} \int_0^\eta \frac{\rho_e^*}{\rho^*}\, d\eta \tag{45}$$

where $y_m^* = y_m L^*$ is the dimensional mean-flow normal coordinate, and $y_m$ follows from Eq. (2) as

$$y_m = \frac{\sqrt{2\xi/Re}}{u_e} \int_0^\eta \frac{1}{\rho}\, d\eta \tag{46}$$

For the case of self-similar flows, $\rho_e = 1$, $u_e = 1$, and $\mu_e = 1$; thus, it follows from Eq. (1) that $\xi = x$. Then Eq. (45) becomes

$$y = \sqrt{2} \int_0^\eta Q\, d\eta \tag{47}$$

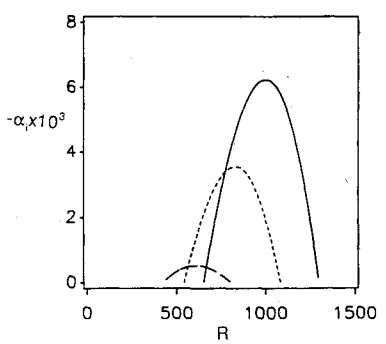


**Fig. 4 Variation of the growth rate with streamwise position for three freestream Mach numbers when $F = 45 \times 10^{-6}$ in case of zero pressure gradient: ——, $M_\infty = 0.0$; . . ., $M_\infty = 1.0$; – – –, $M_\infty = 2.0$.**

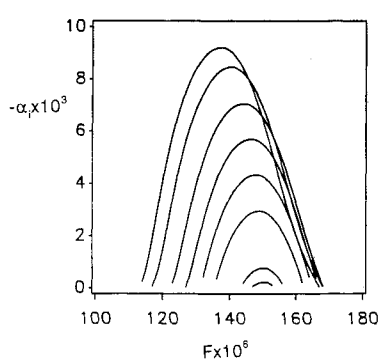


**Fig. 5 Variation of the growth rate of two-dimensional second-mode waves with frequency for different pressure gradients ($M_e = 4.5$ at $R = 1500$). The values of $n$, proceeding downward, are −0.225, −0.2, −0.15, −0.1, −0.05, 0.0, 0.08, and 0.1. The corresponding values of $\beta_0$ are −0.0917, −0.0813, −0.0607, −0.0402, −0.02, 0.0, 0.0313, and 0.0389.**

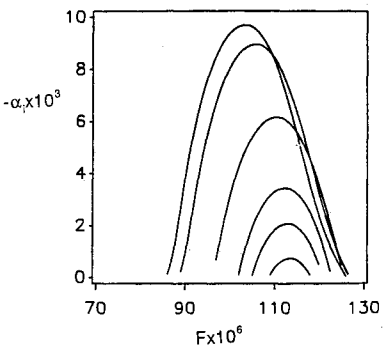


**Fig. 6 Variation of the growth rate of two-dimensional second-mode waves with frequency for different pressure gradients ($M_e = 4.5$ at $R = 2000$). The values of $n$, proceeding downward, are −0.225, −0.2, −0.1, 0.0, 0.05, and 0.1. The corresponding values of $\beta_0$ are −0.0917, −0.0813, −0.0402, 0.0, 0.0196, and 0.0389.**

## V. Results and Discussion

In this study a boundary-layer stability prediction code was developed based on the preceding formulation. The code incorporates both mean-flow and stability calculation routines. The code was tested first for the case of incompressible boundary-layer stability. The results presented in this paper are for $Pr = 0.72$, freestream temperature $T_\infty^* = 120$ K, $P_\infty^* = 0.01373$ atm, and adiabatic wall conditions. As discussed in Sec. II, keeping $T_\infty^*$, and $U_\infty^*$ the same, and varying $L^*$, we can directly compare the influence of the pressure gradient on the stability of the flow at $x = 1.0$. We note that the stagnation temperature will change by changing the Mach number because $T_\infty^*$ is kept constant.

It has been stated earlier that a region of zero pressure gradient ($0 \le x \le 0.2$) is employed in the mean-flow calculations. Then the flow is assumed to undergo either an isentropic compression or an isentropic expansion to the desired edge Mach number. It is assumed that the transition between zero and nonzero pressure gradient regions is such that no shocks are formed. In addition, any shock formed on bodies flying at supersonic speeds is assumed to be far outside the boundary layer. In this case the shock has a little effect on the stability results.[20]

In Fig. 4 we show variation of the growth rate with streamwise location (Reynolds number) for three freestream Mach numbers when $F = 45 \times 10^{-6}$ for the case of a zero pressure gradient. These results are consistent with previous theoretical work.[4] Compressibility is stabilizing, and at the same frequency the locations of the neutral stability points shift to lower values of $R$ as the Mach number increases.

In Fig. 5 we show variation of the growth rate of second-mode (Mack) waves with frequency for different degrees of compression and expansion, all terminating at $M_e = 4.5$. It is clear that favorable pressure gradients are stablizing, whereas adverse pressure gradients are destabilizing. The growth rate increases as the magnitude of the adverse pressure gradient increases, with the peak amplification shifting toward a lower frequency. As in the case of incompressible boundary layers, the band of frequencies receiving amplification widens with an adverse pressure gradient. This trend persists at higher Reynolds numbers, as seen in Fig. 6 for $R = 2000$. However, the band of unstable frequencies shifts to lower values as the Reynolds number increases.

In the preceding cases (Figs. 5 and 6), the freestream Mach number is varied as shown in Fig. 1. The dimensional location where the edge Mach number reaches the desired value of 4.5 varies with the pressure gradient parameter $n$. For example, for $R = 1500$, $L^* = 15.03$ cm when $n = -0.2$, whereas $L^* = 27.16$ cm when $n = -0.1$. For $R = 2000$, $L^* = 26.72$ cm when $n = -0.2$, whereas $L^* = 48.29$ cm when $n = -0.1$.

To investigate the influence of the Mach number, in Fig. 7 we show the effect of the pressure gradient on the growth rate

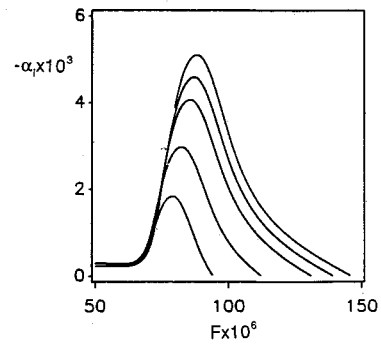


**Fig. 7 Variation of the growth rate of two-dimensional second-mode waves with frequency for different pressure gradients ($M_e = 6.5$ at $R = 1500$). The values of $n$, proceeding downward, are $-0.2$, $-0.15$, $-0.1$, 0.0, and 0.1. The corresponding values of $\beta_0$ are $-0.0429$, $-0.0321$, $-0.0213$, 0.0, and 0.0021.**

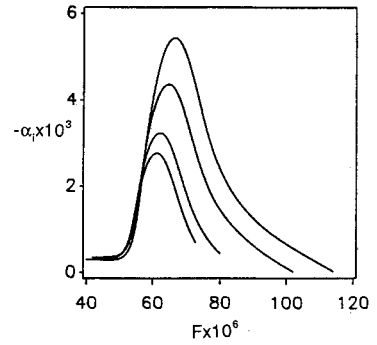


**Fig. 8 Variation of the growth rate of two-dimensional second-mode waves with frequency for different pressure gradients ($M_e = 6.5$ at $R = 2000$). The values of $n$, proceeding downward, are $-0.2$, $-0.1$, 0.0, and 0.04. The corresponding values of $\beta_0$ are $-0.0429$, $-0.0213$, 0.0, and 0.00844.**

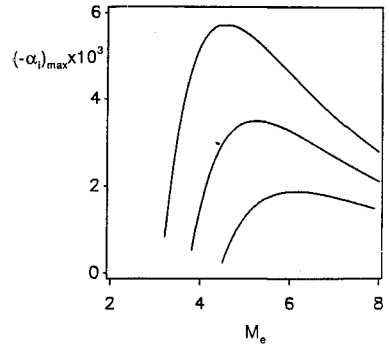


**Fig. 9 Variation of the maximum growth rate of two-dimensional second-mode waves with Mach number for favorable ($n = 0.1$), adverse ($n = -0.1$), and zero pressure gradients at $R = 1500$.**

of second-mode waves when $M_e = 6.5$ at $R = 1500$. As in the case of $M_e = 4.5$, favorable pressure gradients are stabilizing, whereas adverse pressure gradients are destabilizing. The peak amplification decreases and the band of frequencies receiving amplification decreases as the presure gradient increases. However, as the pressure gradient decreases, the peak amplitude shifts to a higher rather than to a lower frequency, in contrast to the case shown in Fig. 5 for $M_e = 4.5$. These trends persist for the Reynolds number ranges investigated (1500–2000), as shown in Fig. 8. The low-frequency regions in Figs. 7 and 8 are the regions where the second- and first-mode waves merge. For the case of zero pressure gradient, Mack[4] showed that at high Mach numbers ($M_\infty = 4.8$) the merging takes place while the waves are amplified, whereas at slightly lower Mach numbers ($M_\infty = 4.5$) it takes place while the waves are damped. This explains the difference in the trends in the low-frequency regions of Figs. 7 and 8 ($M_e = 6.5$) on one hand and Figs. 5 and 6 ($M_c = 4.5$) on the other hand. However, it is not clear why the frequencies corresponding to the peak amplification shift differently at $M_e = 4.5$ and $M_e = 6.5$. We also note from Figs. 7 and 8 that waves with frequencies within the merging region are very insensitive to the pressure gradient parameter.

In Fig. 9 we show variation of the maximum growth rate (maximized over all frequencies) of the two-dimensional second-mode waves with Mach number for three pressure gradients. It is clear that the effect of pressure gradients on changing the maximum growth rates of second-mode waves decreases with increasing Mach number. Also, adverse pressure gradients cause second-mode instability waves to become amplified at lower values of the Mach number. These modes were confirmed to be second-mode waves at these low values of Mach numbers by examination of their eigenfunctions.

The maximum growth rates produced by pressure gradients relative to the maximum amplification rates in the case of zero pressure gradient of Figs. 5–9 are found to vary (see Figs. 10

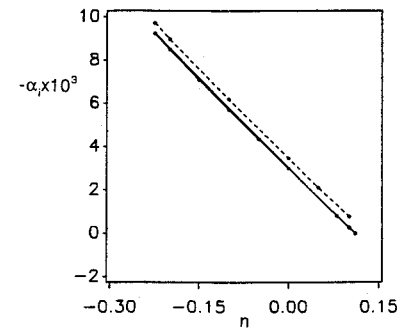


**Fig. 10 Variation of the maximum growth rate of two-dimensional second-mode waves with the pressure gradient parameter $n$ at $M_c = 4.5$: ——, $R = 1500$; . . ., $R = 2000$.**

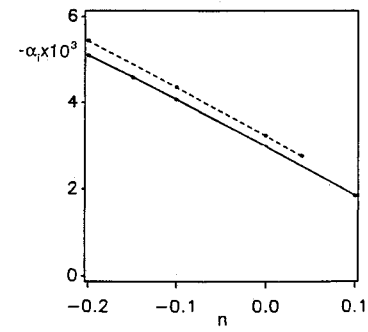


**Fig. 11 Variation of the maximum growth rate of two-dimensional second-mode waves with the pressure gradient parameter $n$ at $M_c = 6.5$: ——, $R = 1500$; . . ., $R = 2000$.**

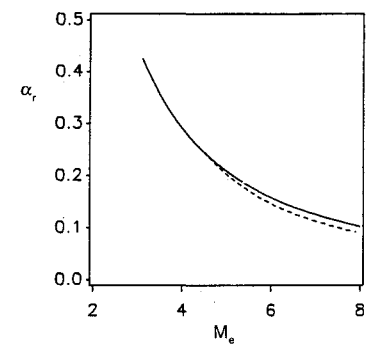


**Fig. 12 Variation of the wave numbers corresponding to the data of Fig. 9: ——, $n = -0.1$; . . ., $n = 0.1$.**

and 11) almost linearly with $n$. This result was found to hold for all of the Mach and Reynolds numbers investigated. It is very significant because it implies that one can calculate the maximum growth rate for any value of $n$ once it is known at two different values (regions close to separation may behave differently).

To fully document the data shown in Fig. 9, in Figs. 12 and 13, we plot variations of the wave number and frequency corresponding to the maximum growth rates shown in Fig. 9. Figure 13 shows that the peak amplification is shifted to a lower frequency as the pressure gradient is decreased when the Mach number is below $M_e \approx 4.5$ and is shifted to a higher frequency when $M_e > 4.5$. These results are consistent with those shown in Figs. 5 and 6.

Turning to the effect of pressure gradient on two-dimensional and three-dimensional first-mode waves, we show in Figs. 14 and 15 the growth rates for adverse, favorable, and zero pressure gradients. A comparison of Fig. 14 for the case of two-dimensional waves with Fig. 15 for the case of three-dimensional waves shows that, for the conditions investigated, oblique first-mode waves are more affected by adverse pressure gradients than two-dimensional first-mode waves. The rate of change in the maximum growth rate for the three-dimensional case is much higher than that for the two-dimensional case.

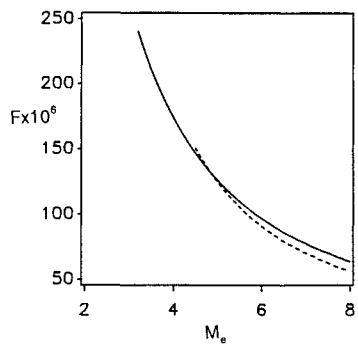


**Fig. 13 Variation of the wave numbers corresponding to the data of Fig. 9: ——, $n = -0.1$; . . ., $n = 0.1$.**

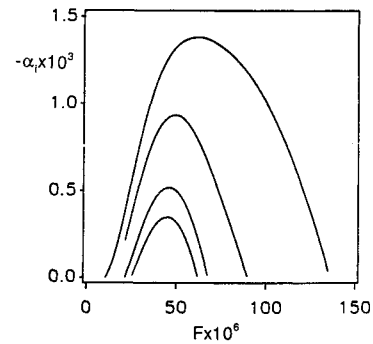


**Fig. 14 Variation of the growth rate of two-dimensional first-mode waves with frequency for four pressure gradients ($M_e = 2.0$ at $R = 600$). The values of $n$, proceeding downward, are $-0.1$, $-0.05$, 0.0. and 0.02.**

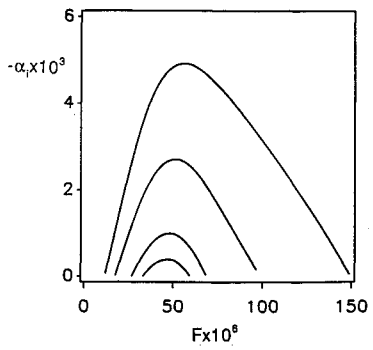


**Fig. 15 Variation of the growth rate of three-dimensional first-mode waves with frequency for four pressure gradients ($M_e = 2.0$, $R = 600$, $\beta = 0.145$). The values of $n$, proceeding downward, are $-0.1$, $-0.05$, 0.0. and 0.02.**

## VI. Closure

The effect of pressure gradient on the stability of compressible boundary layers is investigated by using a viscous analysis. The pressure gradient is generated by using a potential flow corresponding to a power law edge Mach number distribution of the form $M_e = cx^n$. Stability calculations are presented for different Mach and Reynolds numbers and different values of $n$. The results indicate that two-dimensional second-mode waves can be stabilized with favorable pressure gradients and destabilized by adverse pressure gradients. The maximum growth rate produced by pressure gradients varies almost linearly with $n$. Consequently, the maximum growth rate at any pressure gradient can be approximated by using the maximum growth rates calculated for two pressure gradients corresponding to two different values of $n$.

The results show that the effectiveness of favorable pressure gradients in LFC decreases at hypersonic Mach numbers. Stability calculations for first-mode waves indicate that three-dimensional first-mode waves are much more affected by pressure gradients than two-dimensional first-mode waves. In the region where the second mode merges with the first mode, the waves are very insensitive to variations in the pressure gradient.

## Appendix: Nonzero Elements of Matrix $A(y)$

$$a_{12} = a_{56} = a_{78} = 1$$

$$a_{21} = \alpha^2 + \beta^2 - i\hat{\omega}R/\mu_m T_m$$

$$a_{22} = -D\mu_m/\mu_m$$

$$a_{23} = -i\alpha(m+1)DT_m/T_m - i\alpha D\mu_m/\mu_m + RDu_m/\mu_m T_m$$

$$a_{24} = i\alpha R/\mu_m + (m+1)\gamma M_e^2 \alpha\hat{\omega}$$

$$a_{25} = -\alpha(m+1)\hat{\omega}/T_m - D(\mu_m' Du_m)/\mu_m$$

$$a_{26} = -\mu_m' Du_m/\mu_m$$

$$a_{31} = -i\alpha$$

$$a_{33} = DT_m/T_m$$

$$a_{34} = i\gamma M_e^2 \hat{\omega}$$

$$a_{35} = -i\hat{\omega}/T_m$$

$$a_{37} = -i\beta$$

$$a_{41} = -i\chi\alpha(rDT_m/T_m + 2D\mu_m/\mu_m)$$

$$a_{42} = -i\chi\alpha$$

$$a_{43} = \chi[-\alpha^2 - \beta^2 + i\hat{\omega}R/\mu_m T_m + rD^2 T_m/T_m + rD\mu_m DT_m/\mu_m T_m]$$

$$a_{44} = -i\chi r\gamma M_e^2[\alpha Du_m - \hat{\omega}DT_m/T_m - \hat{\omega}D\mu_m/\mu_m]$$

$$a_{45} = i\chi[r\alpha Du_m/T_m + \mu_m'\alpha Du_m/\mu_m - r\hat{\omega}D\mu_m/\mu_m T_m]$$

$$a_{46} = -i\chi r\hat{\omega}/T_m$$

$$a_{47} = -i\chi r\beta DT_m/T_m - 2i\chi\beta D\mu_m/\mu_m$$

$$a_{48} = -i\chi\beta$$

$$a_{62} = -2(\gamma-1)M_e^2 PrDu_m$$

$$a_{63} = -2i(\gamma-1)M_e^2 Pr\alpha Du_m + RPrDT_m/\mu_m T_m$$

$$a_{64} = i(\gamma-1)M_e^2 PrR\hat{\omega}/\mu_m$$

$$a_{65} = \alpha^2+\beta^2 - iRPr\hat{\omega}/\mu_m T_m - (\gamma-1)M_e^2 Pr\mu_m'(Du_m)^2/\mu_m - D^2\mu_m/\mu_m$$

$$a_{66} = -2D\mu_m/\mu_m$$

$$a_{83} = -i(m+1)\beta DT_m/T_m - i\beta D\mu_m/\mu_m$$

$$a_{84} = (m+1)\gamma M_e^2\beta\hat{\omega} + i\beta R/\mu_m$$

$$a_{85} = -(m+1)\beta\hat{\omega}/T_m$$

$$a_{87} = \alpha^2+\beta^2 - i\hat{\omega}R/\mu_m T_m$$

$$a_{88} = -D\mu_m/\mu_m$$

where

$$\hat{\omega} = \omega - \alpha u_m, \qquad \chi = [R/\mu_m - ir\gamma M_e^2\hat{\omega}]^{-1}$$

$$r = m+2, \qquad m = \lambda_m/\mu_m$$

## Acknowledgments

This work was supported by the Office of Naval Research under Contract N00014-85-K-0011/NR 4325201. The assistance of Ahmad Abdelnaser is gratefully appreciated.

## References

[1]Schubauer, G. B, and Skramstad, H. K., "Laminar Boundary Layer Oscillations and Transition on a Flat Plate," NACA Rept. 909, 1948.

[2]Obremski, H. J., Morkovin, M. V., Landahl, M., Wazzan, A. R., Okamura, T. T., and Smith, A. M. O., "A Portfolio of Stability Characteristics of Incompressible Boundary Layers," AGARD Rept. 134, 1969.

[3]van Driest, E. R., and Blumer, C. B., "Boundary Layer Transition: Freestream Turbulence and Pressure Gradient Effects," *AIAA Journal,* Vol. 1, No. 6, 1963, pp. 1303–1306.

[4]Mack, L. M., "Boundary-Layer Stability Theory," Jet Propulsion Lab., Pasadena, CA, Doc. 900-277, Rev. A, 1969.

[5]Lysenko, V. I., and Maslov, A. A., "The Effect of Cooling on Supersonic Boundary-Layer Stability," *ASME Journal of Fluid Mechanics,* Vol. 147, 1984, pp. 39–52.

[6]Gasperas, G., "Effect of Wall Temperature Distribution on the Stability of the Compressible Boundary Layer," AIAA Paper 89-1894, 1989.

[7]Malik, M. R., "Prediction and Control of Transition in Hypersonic Boundary Layers," *AIAA Journal,* Vol. 27, No. 11, 1989, pp. 1487–1493.

[8]Masad, J. A., Nayfeh, A. H., and Al-Maaitah, A. A., "Effect of Heat Transfer on the Stability of Compressible Boundary Layers," *Computers and Fluids,* Vol. 21, No. 1, 1992, pp. 43–61.

[9]Masad, J. A., Nayfeh, A. H., and Al-Maaitah, A. A., "Effect of Suction on the Stability of Supersonic Boundary Layers. Part II. First-Mode Waves," *ASME Journal of Fluids Engineering,* Vol. 113, 1991, pp. 598–601.

[10]Al-Maaitah, A. A., Nayfeh, A. H., and Masad, J. A., "Effect of Suction on the Stability of Supersonic Boundary Layers. Part I. Second-Mode Waves," *ASME Journal of Fluids Engineering,* Vol. 113, No. 4, 1991, pp. 591–597.

[11]Mack, L. M., "Boundary-Layer Linear Stability Theory," AGARD Rept 709, 1984.

[12]Nayfeh, A. H., "Stability of Compressible Boundary Layers," Transonic Symposium: Theory, Application, and Experiment, NASA Langley, Hampton, VA, April 19–21, 1988, NASA CP 3020, Vol. I, Pt. 1, pp. 629–690.

[13]Shapiro, N. M., "Effect of Pressure Gradient and Heat Transfer on the Stability of the Compressible Laminar Boundary Layers," *Journal of the Aeronautical Sciences,* Vol. 23, 1956, pp. 81–83.

[14]Weil, H., "Effect of Pressure Gradient on Stability and Skin Friction in Laminar Boundar Layers in Compressible Fluids," *Journal of the Aeronautical Sciences,* Vol. 18, 1951, pp. 311–318.

[15]Fitzhugh, H. A., "Numerical Studies of the Laminar Boundary Layer for Mach Numbers up to 15," *Journal of Fluid Mechanics,* Vol. 36, Pt. 2, 1969, pp. 347–366.

[16]Blottner, F. G., "Investigation of Some Finite-Difference Techniques for Solving the Boundary Layer Equations," *Computer Methods in Applied Mechanics and Engineering,* Vol. 6, 1975, pp. 1–30.

[17]Levy, S., "Effect of Large Temperature Changes (Including Viscous Heating) Upon Laminar Boundary Layers with Variable Free-Stream Velocity," *Journal of the Aeronautical Sciences,* Vol. 21, 1954, pp. 459–474.

[18]Cohen, C. B., and Reshotko, E., "Similar Solutions for the Compressible Laminar Boundary Layer with Heat Transfer and Pressure Gradient," NACA Rept. 1293, 1956.

[19]Pereyra, V., "PASVA3," *Lecture Notes in Computer Science,* Vol. 76, edited by B. Childs, M. Scott, J. W. Daniel, E. Denman, and P. Nelson, Springer-Verlag, Berlin, 1976, p. 67.

[20]Chang, C.-L., Malik, M. R., and Hussaini, M. Y., "Effects of Shock on the Stability of Hypersonic Boundary Layers," AIAA Paper 90-1448, 1990.